ELSEVIER

Polymer 41 (2000) 2543–2555

polymer

Comparison of compatibilizer effectiveness for PET/PP blends: their mechanical, thermal and morphology characterization

C.P. Papadopoulou, N.K. Kalfoglou*

Department of Chemistry, University of Patra, 26500 Patra, Greece

Received 9 February 1999; received in revised form 1 June 1999; accepted 14 June 1999

Abstract

The compatibilizing efficiency for PET/PP blends was examined using tensile testing, dynamic mechanical analysis (DMA), differential scanning calorimetry (DSC) and scanning electron microscopy of crycrofractured surfaces before and after etching. Compatibilizers used were maleic anhydride modified, PP (PP-*g*-MA), LLDPE (LLDPE-*g*-MA) and hydrogenated SBS block copolymer (SEBS-*g*-MA). Large deformation behavior of aged blends indicated that SEBS-*g*-MA performed best by far. However, addition of a thermoplastic polyolefin alloy (TPO), PP/ethylene–propylene copolymer, increased the compatibilizing efficiency of PP-*g*-MA to a level comparable to that of SEBS-*g*-MA. Improved efficiency of SEBS-*g*-MA and PP-*g*-MA + TPO compared to PP-*g*-MA or LLDPE-*g*-MA is attributed to better emulsification of the former at the interface, reduced migration of PP-*g*-MA into the PP phase and retardation of PET crystallization in the presence of the elastomeric additive. In addition, the elastomeric compatibilizers absorb more efficiently, the stresses developed at the PET/PP interface.

Keywords: PET/PP alloys; Compatibilization; Compatibilizer effectiveness

1. Introduction

Among thermoplastic polymer alloys the combination of polypropylene (PP) with poly(ethylene terephthalate) (PET) offers some advantages over the pure components. PET may enhance the stiffness of PP at higher temperatures while the polyolefin could facilitate crystallization of PET by heterogeneous nucleation further raising blend stiffness. In addition, the lower permeability of PET towards water vapor and oxygen could be usefully utilized in packaging materials if the morphology of the alloy is optimized. Also the hydrophobic nature of the polyolefin may in principle reduce moisture sensitivity of the polyester and facilitate its crystallization. This is of significance in processing and molding operations. In addition to property diversification, utilizing thermoplastics available through recycling technology may contribute to the abatement of environmental pollution and resource conservation.

Previous studies on this binary blend include the work of Bataille et al. [1] who studied tensile properties and water vapor permeability of noncompatibilized PET/PP in the complete range of composition, and one composition at several compatibilizer levels. The compatibilizer was a PP–acrylic acid copolymer (PP-*g*-AA). The improvement of mechanical properties was marginal, and as expected permeability of PP towards oxygen was reduced with the addition of PET. The same compatibilizer was employed by Xanthos et al. [2] who also added a transesterification catalyst. A complete characterization was carried out to evaluate compatibilization and the limited strength reinforcement observed was attributed to improved components dispersion and possibly physical interactions. As Lambla pointed out [3] the use of acrylic acid as the active functionality of a compatibilizer has the disadvantage of being kinetically slow when esterified with the terminal OH groups of the polyester. Successful compatibilization as evidenced by large deformation mechanical behavior and morphology was reported by Ballauri et al. [4], using a maleic-anhydride modified hydrogenated SBS block copolymer (SEBS-*g*-MA). A more complete study on the same system compatibilized with SEBS, or SEBS-*g*-MA, or glycidyl methacrylate modified SEBS (SEBS-*g*-GMA) at one ternary composition, was reported by Heino et al. [5]; their report covered morphology, mechanical and rheological properties. In a more recent paper Morye et al. [6] reported on the rheology, mechanical properties and permeability to oxygen and water vapor of PET/PP blends in a limited

* Corresponding author. Tel.: +30-61-997102; fax: +30-61-997122.
E-mail address: n.kalfog@chemistry.upatras.gr (N.K. Kalfoglou)

0032-3861/00/$ - see front matter
PII: S0032-3861(99)00442-5

composition range with increased levels of PP and using ethylene–vinylacetate (EVA) and EVA-*g*-MA as compatibilizers. Though compatibilization was inferred on the basis of blend melt rheology, mechanical properties did not support this contention. As to results on permeability, the conclusions were ambiguous since EVA itself may offset the barrier properties of PET if the latter is present in small amounts in the blend.

Related to the PET/PP binary blends are also reports on the blends of poly(butylene terephthalate) (PBT)/PP and PET/PE. Of the former, the work of Tsai and Chang [7] examined the compatibilizing efficiency of ethylene-*co*-glycidyl methacrylate (E–GMA) both with and without the addition of a transesterification catalyst. For the same binary blend Lambla and coworkers [3] analyzed the compatibilizing efficiency of various in situ formed compatibilizers containing MA, AA or the GMA functionality which would react with the terminal OH and/or COOH groups of PBT. Mixing protocol was also examined. On the basis of large deformation behavior, PP-*g*-GMA was shown to be most effective, and in a single step mixing procedure. Application of PP-*g*-GMA for the compatibilization of the PP/PC blend was recently studied by Jighua et al. [8]. They reported reduction of the interfacial tension of the compatibilized blend, leading to size reduction of the dispersed phase (PC) and improvement of large deformation mechanical behavior of the polymer alloy. Compatibilization was attributed to the reaction of the GMA functionality with the terminal OH groups of the PC, in analogy to the compatibilization of PET/polyolefin blends. Work on the compatibilization of PE/PET is quite extensive and will not be cited since it is adequately summarized in recent papers [9,10].

In this work we compare the compatibilizing efficiency for PET/PP blends of various compatibilizers; namely, SEBS-*g*-MA, PP-*g*-MA and LLDPE-*g*-MA.

Tensile, dynamic mechanical, thermal and morphological properties were examined. Emphasis is given on the effect of aging on large deformation behavior since considerable property differentiation was observed depending on the compatibilizer used. Results were interpreted in terms of varying phase microstructure, mutual component wettability and crystallinity development in the blend.

2. Experimental

2.1. Materials and specimen preparation

PET was extrusion grade obtained from Akzo b.v. (Arnite DO2 300). It was reported to have predominantly terminal hydroxyl groups $M_n = 23\,500$ g mol^{-1}, $T_m = 252$°C and an amorphous product density of 1.34 g cm^{-3}. PP was obtained from APPRYL S.N.C. Co (3020BN1). It is a blow molding and thermoforming grade with density 0.905 g cm^{-3} and MFI 1.9 (230°C/2.16 kg).

The compatibilizers used were: SEBS-*g*-MA (Kraton FG-1901X) a Shell Chemical Co. product. It contained 29 wt% styrene; the MW of the styrene block was 7000, that of the ethylene–butylene block 37 500 and the MA content was 1.84 wt% [11]. The unmodified SEBS was also used; it was donated by Shell Chemical Co., (Kraton G-1652). The PP-*g*-MA (PB 3150) used was donated by Uniroyal Chemical, Specialty Chemicals Div., UK, and was reported to have 0.32 wt% MA. The modified linear low density PE, LLDPE-*g*-MA (41E558) was obtained from Du Pont de Nemours Co. and had ca. 0.25 wt% MA. To improve the compatibilizing effectiveness of PP-*g*-MA, use was made of a thermoplastic polyolefin alloy-PP mixed at equal proportion with ethylene–propylene copolymer (EPM). It was donated by Esso Chemicals, Europe (Vistaflex 911). Its density was 0.89 g cm^{-3} and MFI 18 (230°C, g/10 min). In the following it will be identified as TPO.

PET was dried at 150°C for 12 h in dynamic vacuo. PP was dried at 80°C for 24 h and compatibilizers were dried at 60°C overnight in dynamic vacuum. The dried materials were blended under argon atmosphere in a home-made stainless steel bob-and-cup type of mixer previously described [12]. Based on the optimization of ultimate tensile properties, strength (σ_b) and elongation (ϵ_b%), mixing was carried out in a single step at 275°C for 20 min. The compositions prepared will be described for each case as required. Films were obtained by compression molding between Teflon sheets at 275°C followed by pressure release and quenching to 0°C.

2.2. Apparatus and procedures

Tensile tests were performed at a crosshead speed of 10 cm min^{-1}, at 23°C according to ASTM D882 using a J.J. Tensile Tester type 5001 and rectangular strips measuring $6.0 \times 0.65 \times 0.25$ cm^3.

Dynamic mechanical analysis (DMA) data, storage modulus E' and loss modulus E'', were obtained at 10 Hz with RSA II mechanical spectrometer of Rheometric Scientific Ltd. Specimen dimensions were $2.3 \times 0.5 \times 0.015$ cm^3. Some binary blends (PET/SEBS-*g*-MA and PET/PP-*g*-MA) were tested at 110 Hz using Rheovibron (DDV III-C).

Differential scanning calorimetry (DSC) measurements were carried out using the DSC (SP +) equipped with the AutoCool accessory from Rheometric Scientific Ltd. Nominal weight was 10 mg, and the thermal cycling applied for the crystallinity determination of the PET/SEBS-*g*-MA/PP blends was 25 → 290°C with 20°C/min heating rate, quenching to 25°C and heating up to 290°, at the same heating rate.

The half time $t_{1/2}$ of the crystallization process and the crystallinity of the PET/PP-*g*-MA + TPO/PP blends was determined according to the following procedure: the samples were held as melt for 5 min and cooled at 10°C/min to the crystallization temperature T_c. All the

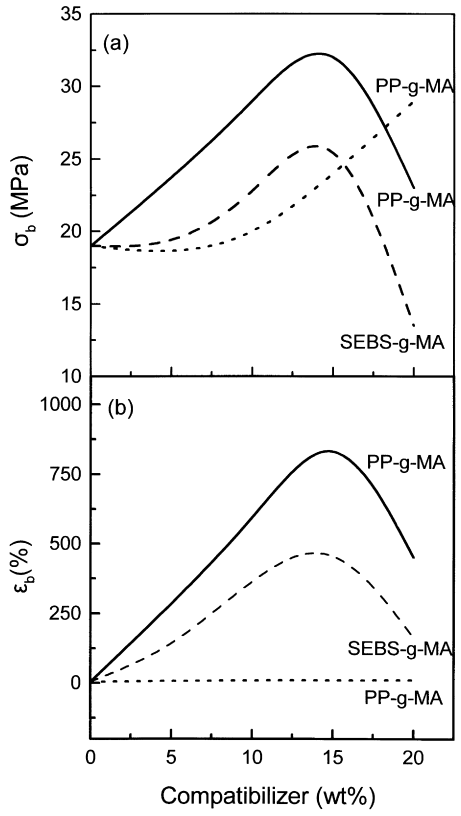

Fig. 1. Effect of compatibilizer type and content on, (a) tensile strength, (b) ultimate elongation of ternary blends at PET/PP 2/1 ratio, after 1 day. (⋯) with PP-*g*-MA aged for 10 days.

Table 1
Ultimate tensile properties of blends (quenched and aged for 10 days)

Composition	σ_y (MPa)[a]	σ_b (MPa)	ϵ_b (%)
a. PET/PP			
2/1	–	14 ± 1	5 ± 1
1/1	–	17 ± 3	5 ± 1
1/2	–	19 ± 2	5 ± 1
b. PET/SEBS-*g*-MA/PP			
70/30/0	18 ± 1	24 ± 2	407 ± 30
70/30/0[b]	–	12 ± 4	24 ± 3
30/70/0	–	14 ± 1	891 ± 45
56.7/15/28.3	19 ± 1	25 ± 4	547 ± 124
42.5/15/42.5	12 ± 1	14 ± 2	360 ± 160
28.3/15/56.7	12 ± 1	19 ± 2	722 ± 104
c. PET/PP-*g*-MA + TPO/PP			
53.3/15 + 5/26.7	27 ± 2	28 ± 5	744 ± 250
40/15 + 5/40	24 ± 1	19 ± 3	407 ± 73
26.7/15 + 5/53.3	–	18 ± 4	12 ± 7
d. PET/LLDPE-*g*-MA/PP			
56.7/15/28.3	–	23 ± 2	13 ± 3
42.5/15/42.5	–	17 ± 1	8 ± 1
28.3/15/56.7	–	16 ± 1	13 ± 5

[a] Yield stress.
[b] PET/SEBS/PP.

experiments were performed under a constant flow of dry nitrogen.

Optical micrographs with phase contrast and crossed polar arrangements were obtained with an Olympus BH-2 microscope.

Scanning electron microscopy was carried out on a JEOL model JSM-500 instrument. Cryofractured or etched surfaces were examined at a tilt angle of 30°. Warm toluene was used to remove SEBS-*g*-MA and cyclohexane to remove TPO (2 h treatment for both).

3. Results

3.1. Tensile properties

Large deformation behavior in terms of σ_b and ϵ_b% is summarized in Fig. 1 for two types of compatibilizers at different contents at a constant PET/PP ratio (2/1). These data indicate an optimum compatibilizer level of ca 10–15 wt% for all nonaged blends. For the PET/PP-*g*-MA/PP ternary ductility reduction, see Fig. 1(b), attributed to physical aging is observed at all compatibilizer levels within 10 days with a concomitant increase of strength, see Fig. 1(a). Table 1 gives additional ultimate tensile data on aged samples using four types of compatibilizers at a constant level at different PET/PP ratios.

Since the adverse effect caused by aging in the case of PET/PP-*g*-MA/PP, was attributed to lack of ductility at the interface and possibly to an unstable morphology, TPO was added. The improvement attained is shown in Fig. 2, where the relative stability against aging is shown for four compatibilizers; SEBS-*g*-MA and PP-*g*-MA plus 5 wt% TPO give blends with mechanical properties stable towards aging. From the polyolefin-*g*-MA compatibilizers we chose to improve the performance of PP-*g*-MA because of its chemical similarity to TPO and to one of the main blend components (PP). Consideration of the data in Figs. 1 and 2 and inspection of Table 1 shows that in general, polyolefin-*g*-MA compatibilizers are inferior to SEBS-*g*-MA compatibilizers unless the TPO additive is used. This is further discussed in the last section. The effect of changing the PET/PP ratio is small and in the case of the polyolefinic compatibilizers their migration into the PP phase complicates any interpretation.

To demonstrate the decisive role of the MA functionality in attaining PET compatibilization, a comparison of PET/SEBS-*g*-MA with PET/SEBS is made in Table 1b. Tensile properties of the latter are typical of an incompatible blend. This is expected since no MA is present to bind PP onto PET via the anhydride/PET terminal hydroxyl reaction [10].

In Table 2 the effect of the mixing protocol is examined for the PET/SEBS-*g*-MA/PP blend. Based on the tensile data reproducibility, one would infer that premixing of PET/SEBS-*g*-MA improves ternary blend performance. This may be attributed to a better dispersal and bonding of

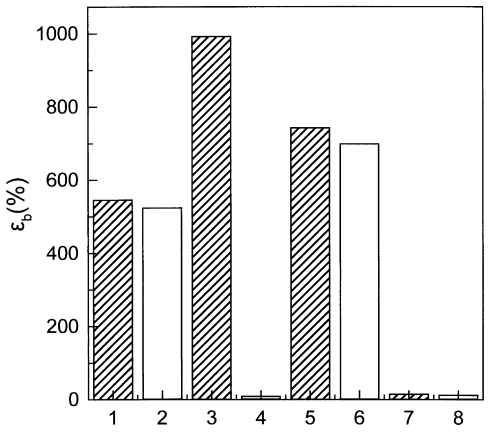

Fig. 2. Effect of compatibilizer type (at 15 wt%), on ultimate elongation of ternary blends at PET/PP 2/1 ratio; (▨) after 1 day; (□) aged for 10 days: bars 1–2, SEBS-*g*-MA; 3–4, PP-*g*-MA; 5–6, PP-*g*-MA + 5 wt% TPO; 7–8, LLDPE-*g*-MA.

SEBS-*g*-MA onto PET during the first mixing step followed by improved wetting of the polyolefinic block of the compatibilizer with PP at the second mixing stage. On the contrary, premixing of PP/SEBS-*g*-MA may dilute the compatibilizer and reduce the amount available for reacting with PET at the final mixing stage.

3.2. Dynamic mechanical properties

3.2.1. Binary PET/compatibilizer blends

D.m.a. spectra on binary blends can provide information on the degree of polymer-compatibilizer interaction and interphase mixing. Viscoelastic spectra of blends in terms of storage E' and loss modulus E'' are given in Figs. 3 and 4 for PET/SEBS-*g*-MA and PET/PP-*g*-MA, respectively. The main component relaxations of PET at 92°C (α) and of SEBS-*g*-MA at −36°C (β) show a small mutual convergence also reported earlier [10]. At high SEBS-*g*-MA contents, see Fig. 3, the PET relaxation disappears and the modulus variation is typical of a phase-inverted system. Overall, the spectra are typical of a polymeric alloy and T_g shifts are attributed to limited interphase mixing.

Table 2
Effect of mixing protocol on the ultimate tensile properties of PET/SEBS-*g*-MA/PP blends (30/10/60) (quenched to 0°C and aged for 10 days)

Protocol	σ_y (MPa)	σ_b (MPa)	ϵ_b (%)
a. One-step mixing, 20 min	16 ± 1	16 ± 2	565 ± 104
b. Mixing of PET/SEBS-*g*-MA, 15 min followed by PP addition and mixing, 5 min	15 ± 2	16 ± 4	503 ± 23
c. Mixing of PP/SEBS-*g*-MA, 15 min followed by PET addition and mixing, 5 min	–	13 ± 3	45 ± 3

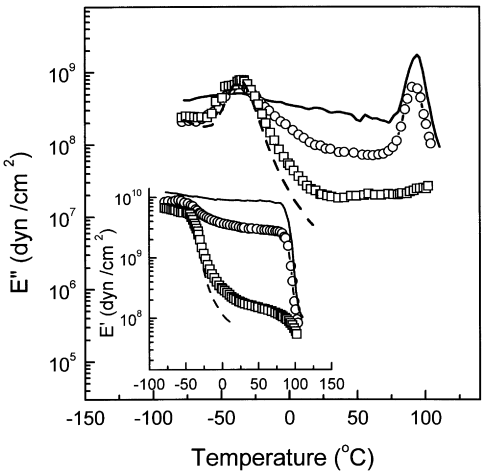

Fig. 3. Temperature dependence of loss modulus E'' of PET/SEBS-*g*-MA blends: (—) 100/0; (○) 70/30; (□) 30/70; (– –) 0/100. Inset: storage modulus E'. Frequency 110 Hz.

3.2.2. Ternary blends

In Fig. 5, DMA spectra are reported for PET/PP (2/1) blends at constant (15 wt%) PP-*g*-MA level, containing varying amounts of the TPO additive. The T_g (PET) shifts considerably (ca 7°C) while modulus variation in Fig. 5(b) indicates an increase of PP stiffness at above ambient temperatures; this was one of the goals of this work. Analogous trends were found for PET/LLDPE-*g*-MA/PP blends and are reported elsewhere [13].

3.3. Thermal properties

The pure component crystallinities of PET/SEBS-*g*-MA/PP blends as determined during the heat-scan of quenched blends are recorded in Table 3a. PET crystallinity is reduced as the PET/PP ratio decreases at constant compatibilizer level, 15 wt%. In two of the ternary blends, PET

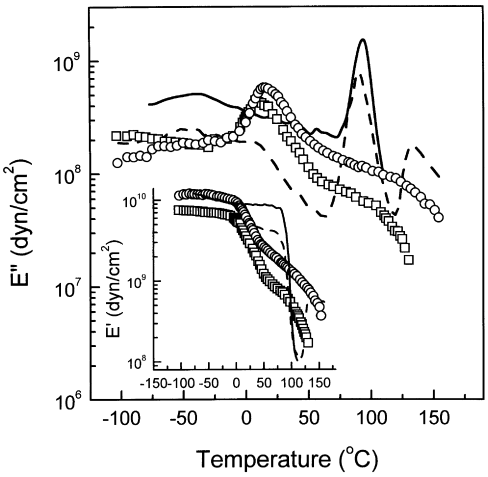

Fig. 4. Temperature dependence of loss modulus E'' of PET/PP-*g*-MA blends: (—) 100/0; (– –) 85/15; (□) 0/100; (○) PP. Inset: storage modulus E'. Frequency 110 Hz.

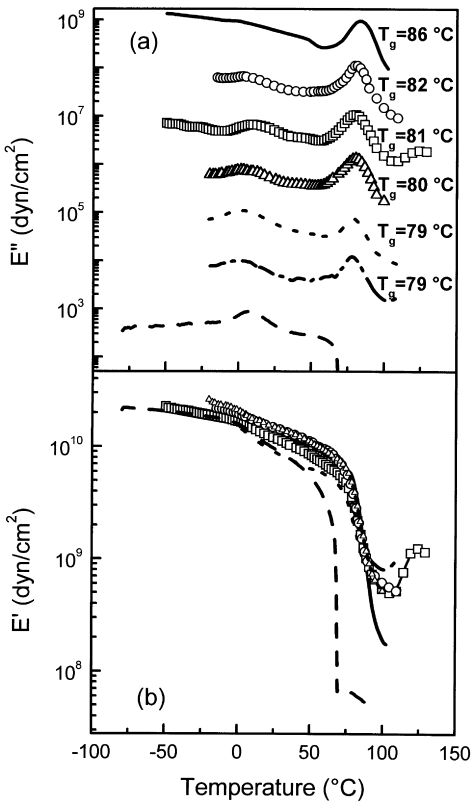

Fig. 5. Temperature dependence of loss modulus E'' of PET/PP-*g*-MA + TPO/PP blends at constant PET/PP ratio (2/1) and 15 wt% PP-*g*-MA and varying contents of TPO: (—) 66.7/0 + 0/33.3; (○) 56.7/15 + 0/28.3; (□) 55.3/15 + 2/27.7; (△) 53.3/15 + 5/26.7; (- -) 50/15 + 10/25; (– · –) 46.7/15 + 15/23.3; (– –) PP. Top spectrum in scale, the rest shifted by one cycle. Frequency 10 Hz.

crystallinity is higher than that of pure PET. This is attributed to heterogeneous nucleation due to the presence of PP crystals in the quenched blends. The decrease of PET crystallinity as the PET/PP ratio decreases is due to the concomitant increase of the SEBS-*g*-MA/PET reaction, the reaction product hindering PET crystallization. PP crystallinity remains essentially constant since it is not involved chemically in the compatibilization reaction. The small reduction of PP crystallinity observed at high PET contents is attributed to the presence of cold crystallized PET. Thus while limited PP crystallinity develops in quenched blends, its full development is hindered during the heat scan due to the hindrance of cold crystallized PET above ca 100°C. Crystallinity development was also examined in the ternary PET/PP-*g*-MA/PP at various PET/PP ratios and constant compatibilizer (15 wt%) and TPO (5 wt%) content during the cooling scan (see Table 3b,c). In Table 3c crystallinity data are recorded for the same ternary at constant PET/PP ratio (2/1) and compatibilizer level (15 wt%) with increasing TPO content. The above results were obtained during a controlled cooling scan to T_c. The trend for PET crystallinity is similar to that observed in Table 3a. Some reduction of PET crystallinity is observed on adding TPO; a possible explanation is proposed below. This is also the case for the PP component, which however crystallizes in the presence of PET crystals. No explanation on the effect of changing the PET/PP ratio can be suggested at present. Also, Table 3c indicates that increasing the TPO content decreases crystallinity levels for both main components. This is attributed to the rubbery nature of TPO, which may decrease the rate of diffusional processes associated with crystallization. This factor may contribute to the aging resistance observed for ternary blends containing TPO. Crystallinity reduction may reflect a decrease of the rate of crystallization in the presence of the TPO additive. Thus crystallinity measurements were carried out to determine the crystallization half-time $t_{1/2}$, defined as the time required for the degree of crystallinity to reach a level of 50%; $t_{1/2}$ was determined using the relationship [14]:

$$t_{1/2} = \frac{T_{ons} - T_{1/2}}{\text{scan rate}(^{\circ}\text{C/min})}$$

where, T_{ons} is the temperature at the crystallization onset and $T_{1/2}$ is the temperature where 50% of sample crystallinity has been attained. The results obtained for the ternary are given in Table 3c and Fig. 6. It is seen that the rate of PET crystallization passes through a minimum at ca. 5 wt% TPO while that of PP at these compositions remains constant. Higher contents of the TPO additive decrease the PP crystallization rate while the effect on PET is in the opposite direction. Decreased crystallization rates may influence crystallinity levels and in this respect the optimum level of TPO seems to be in the range of 5–10 wt%.

3.4. Morphology

3.4.1. Optical microscopy

Phase-contrast micrographs of binary PET/SEBS-*g*-MA blends are shown in Fig. 7(a)–(d). Given the refractive indices of PET ($n_D = 1.64$) and of SEBS-*g*-MA having a lower mean value, at positive phase-contrast, dark areas correspond to PET. Unmodified SEBS is incompatible and poorly dispersed in PET. This is in line with the mechanism of the reactive compatibilization (va.) and the poor tensile properties observed; see Table 1b. Micrographs with crossed polars (Fig. 7(e)–(h)) show well dispersed PET crystallites in the compatibilized blend; micrograph Fig. 7(f). Increase of SEBS-*g*-MA leads to poor dispersal of PET domains while at high compatibilizer content crystallinity development is limited; Fig. 7(h). Good component dispersion is also evident in the ternary blends of PET/SEBS-*g*-MA/PP at various PET/PP ratios, provided that the compatibilizer does not exceed the 10 wt% level; compare Fig. 8(a)–(d) with Fig. 8(e)–(f). In the last micrographs phase separation of the compatibilizer is evident leading to mechanical properties deterioration (see Fig. 1(b)).

Fig. 9 gives phase-contrast micrographs of PET/PP-*g*-MA/PP blends at constant PET/PP ratio (2/1) and compatibilizer level (15 wt%) with varying contents of

Table 3
Crystallinity of PET and PP in ternary blends

Composition	x_c (%)	
	PET[a]	PP[b]
a. PET/SEBS-*g*-MA/PP[c]		
100/0/0	21	—
56.7/15/28.3	30	34
42.5/15/42.5	22	35
28.3/15/56.7	14	37
0/0/100	—	37
b. PET/PP-*g*-MA + TPO/PP[d]		
PET	31	
PP	—	59
PP-*g*-MA		54
TPO		18
56.7/15 + 0/28.3	38	60
53.3/15 + 5/26.7	30	44
40/15 + 5/40	30	57
26.7/15 + 5/53.3	27	46
c. PET/PP-*g*-MA + TPO/PP[d]		
56.7/15 + 0/28.3	38	60
55.3/15 + 2/27.7	31	58
53.3/15 + 5/26.7	30	44
50/15 + 10/25	27	36
46.7/15 + 15/23.3	26	38

[a] $\Delta H_f = 35.5$ cal g^{-1}.
[b] $\Delta H_f = 39.4$ cal g^{-1}. Calculation was based on total PP mass in blends.
[c] Determination of x_c% during heating scan.
[d] Determination of x_c% during cooling scan.

TPO (0–15 wt%). Micrograph Fig. 9(a) shows the poor dispersion of PET/PP blend in the absence of PP-*g*-MA. For the ternary blends, a finer dispersion is obtained at 5 wt% TPO, higher amounts leading to agglomeration of the elastomeric additive; micrographs Fig. 9(e) and (f). At a higher magnification (Fig. 9(g) and (h)) morphological details support the view that the polyolefin envelops the PET phase. This is in line with the observations using SEM and considerations of interfacial tension developed between components; see below.

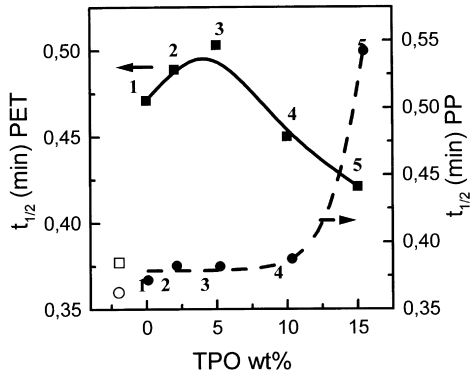

Fig. 6. Crystallization half-time dependence on TPO content of PET and PP in PET/PP-*g*-MA + TPO/PP blends at PET/PP ratio 2/1. Open symbols PET/PP blend.

3.4.2. SEM microscopy

Cryofractured surfaces of blends are shown in Fig. 10. The noncompatibilized PET/PP blend (Fig. 10(a)) shows the smooth craters left in the PET matrix when PP is pulled out during fracture and it is typical of poor interfacial bonding. Addition of compatibilizer leads to ductile fracture (Fig. 10(b)–(d)) however, a more uniform dispersion is obtained when PP-*g*-MA is combined with TPO; compare Fig. 10(c) and (d). Figs. 10(d) and 11 show the effect of varying the TPO content in PET/PP-*g*-MA/PP blends. A 2 wt% addition of TPO leads to drastic morphology improvement, however, small craters are still visible. Increased levels of TPO (>5 wt%) lead to coarsely distributed phases (Fig. 11(b)) and a glassy fracture (Fig. 11(c)). In Fig. 12 fractured and etched surfaces of compatibilized blends are shown. SEBS-*g*-MA was removed with warm toluene and TPO with cyclohexane. The craters in Fig. 12(a) suggest that PP is removed with SEBS-*g*-MA, which concentrates at the PET/PP interface. Removal of interphasial material yields circular gaps surrounding the dispersed PP phase. This is also the case for the TPO additive in PET/PP-*g*-MA/PP blend (see Fig. 12(c)). These results are in line with the findings from phase-contrast microscopy (see Fig. 9(g) and (h)).

4. Discussion

On the basis of large deformation behavior, in particular ϵ_b%, SEBS-*g*-MA is a better compatibilizer than the pure polyolefin compatibilizers tested. However, PP-*g*-MA becomes equally effective in improving and stabilizing tensile properties against aging when combined with TPO.

Improved ultimate tensile properties in compatibilized blends is a characteristic of good interfacial adhesion. This is also supported by small shifts observed in the DMA spectra of binary blends and indirectly by the application of the Kerner mechanics model [15]. For the latter to apply, the basic assumptions are: strongly adhering spherical inclusions in the matrix and negligible interactions between the particles. The model was found to be applicable with PET as a matrix and SEBS-*g*-MA as the dispersed phase as well as the inverted system. Fig. 13 compares the complex modulus $|E^*|$ calculated with Kerner's model with experimental values obtained for the 70/30 and 30/70 PET/SEBS-*g*-MA blends. Given the approximations involved, the prediction is satisfactory, validating the assumption of strong interfacial adhesion.

The improved performance of SEBS-*g*-MA is primarily due to two factors; (i) its chemical structure leading to microphase domains causes it to concentrate at the interface enhancing its emulsifying effectiveness and (ii) the presence of PS blocks prevents its migration and loss into the polyolefin phase, in contrast to a polyolefinic compatibilizer.

A reduced compatibilizer efficiency for a modified PE-*g*-MA compared to SEBS-*g*-MA was also reported in the case

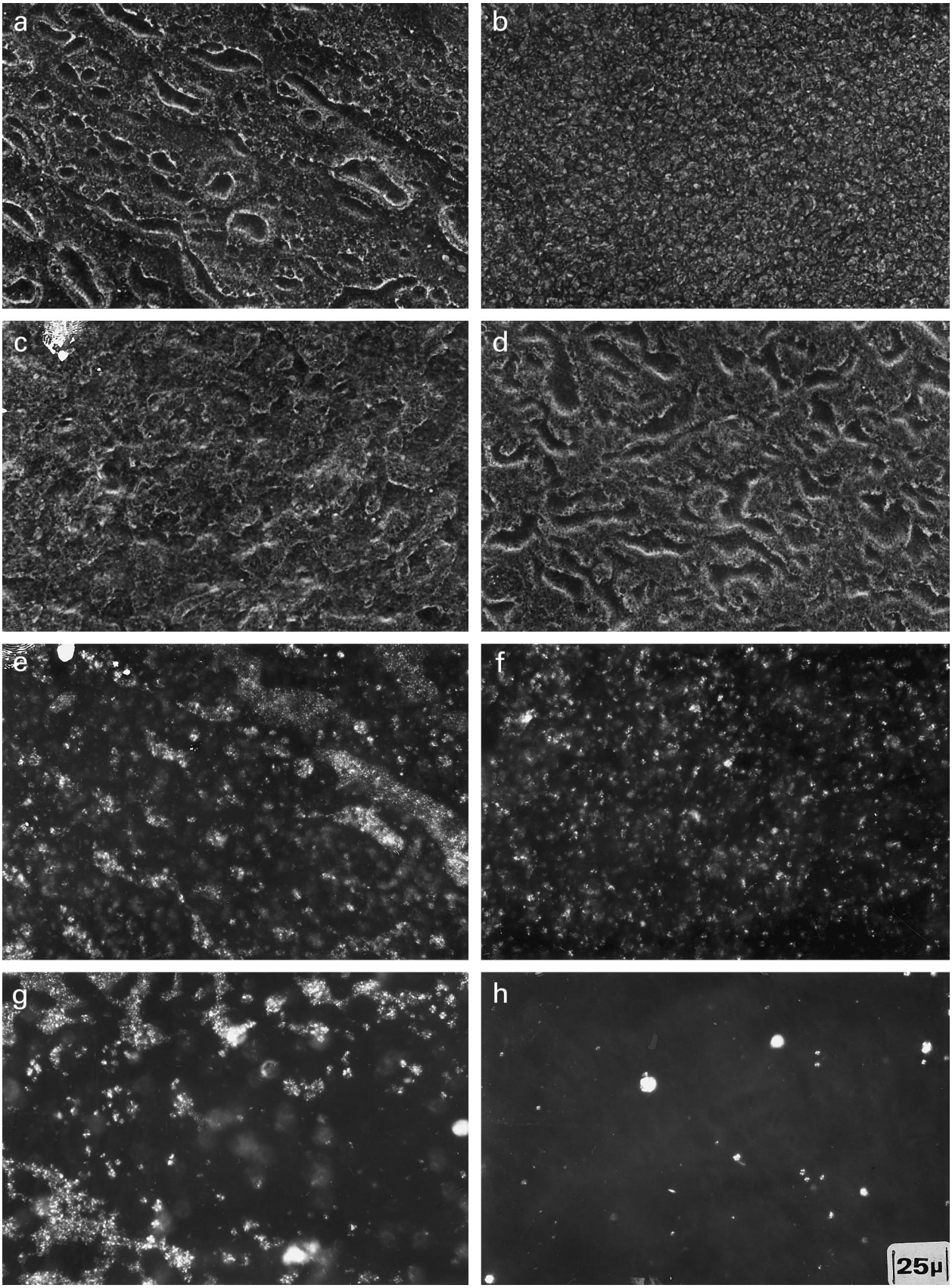

Fig. 7. Phase-contrast micrographs of binary blends; PET/SEBS: (a) 70/30. PET/SEBS-*g*-MA: (b) 70/30; (c) 50/50; (d) 30/70. With crossed polars; PET/SEBS: (e) 70/30. PET/SEBS-*g*-MA: (f) 70/30; (g) 50/50; (h) 30/70.

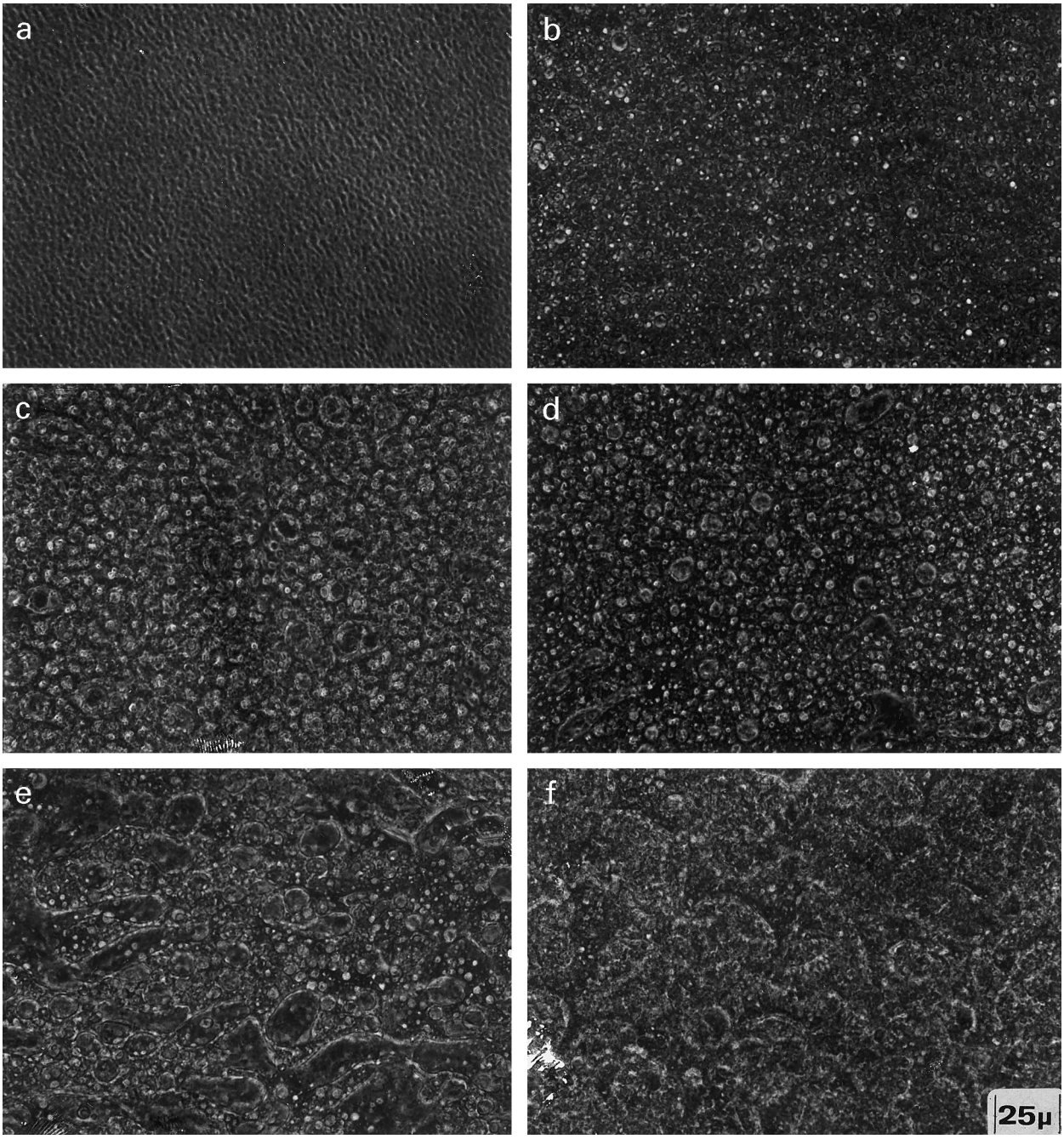

Fig. 8. Phase-contrast micrographs of ternary PET/SEBS-*g*-MA/PP blends, at various compatibilizer levels: (a) 30/10/60; (b) 45/10/45; (c) 63.3/5/31.7; (d) 60/10/30; (e) 56.7/15/28.3; (f) 53.3/20/26.7.

of PET/HDPE blends [10]. Since the EPM component of TPO is insoluble in PP, the thermoplastic additive concentrates at the PET/PP interface increasing the effectiveness of PP-*g*-MA as a compatibilizer; see below. This is supported by the morphological evidence presented and interfacial property considerations between main components. Using the concept of the spreading coefficient Hobbs et al. [16] successfully explained blend morphologies of ternary blends. For components 1, 2 and 3 the spreading coefficient may be defined as:

$$\lambda_{31} = \gamma_{12} - \gamma_{23} - \gamma_{31} \quad (1)$$

For component 3 to spread over dispersed component 1, λ_{31}, should be positive and the corresponding morphology is shown in Fig. 14(a). In all the cases examined with PET or PP as matrix (phase 2), λ_{31}, was calculated to be positive only when TPO (phase 3) was spreading over the dispersed phase.

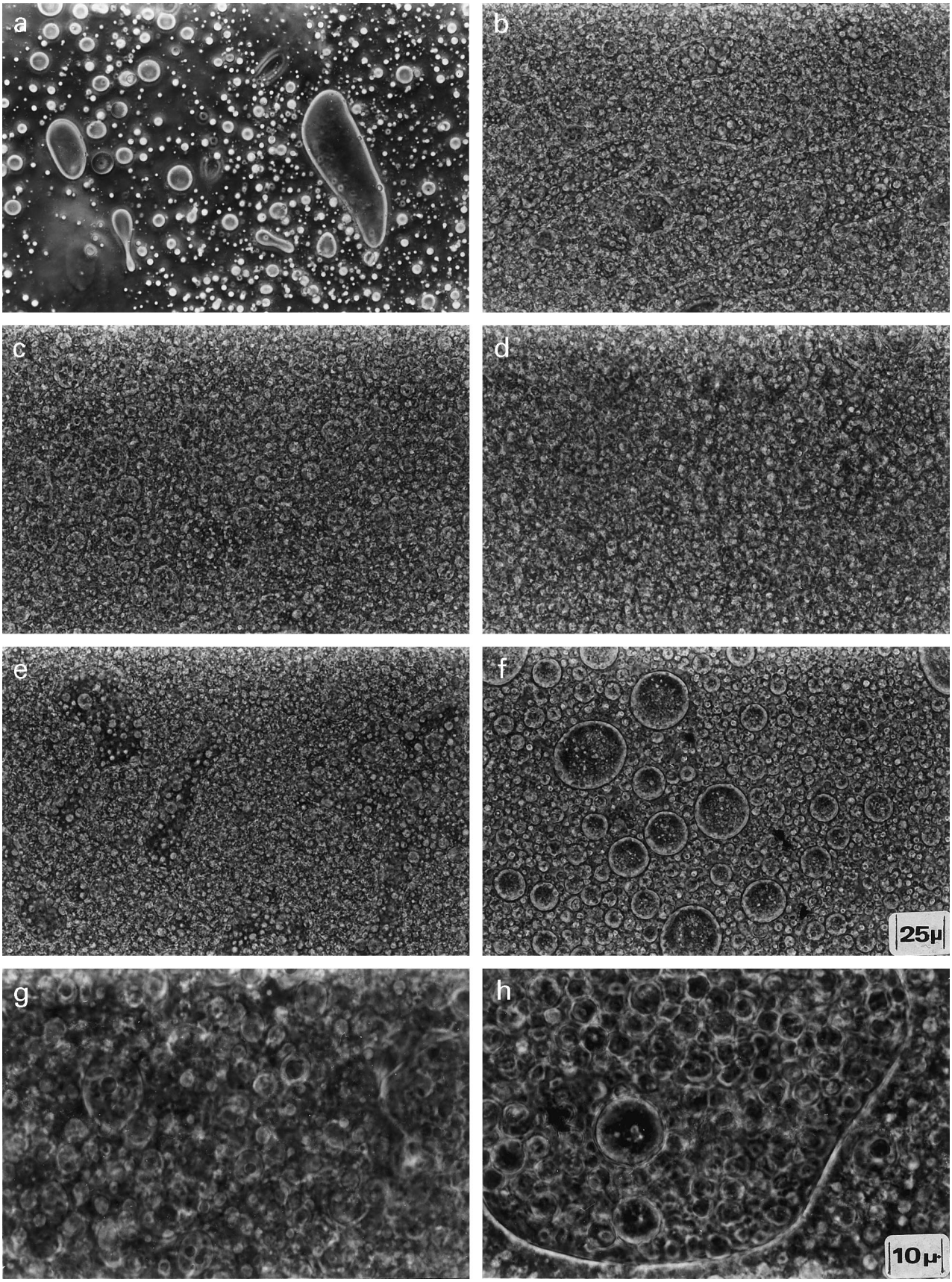

Fig. 9. Phase-contrast micrographs of PET/PP-*g*-MA + TPO/PP blends at PET/PP ratio 2/1 and 15 wt% PP-*g*-MA with varying TPO contents: (a) PET/PP, 2/1; (b) TPO 0 wt%; (c) 2 wt%; (d) 5 wt%; (e) 10 wt%; MA: (f) 15 wt%. At higher magnification: (g) 10 wt%; (h) 15 wt%.

A similar result is obtained by application of the criterion of a free energy minimum G_{min} associated with a given morphology of a multicomponent polymer alloy at equilibrium, proposed by Meier and coworkers [17]. It was shown that G is minimized, thus a stable morphology is obtained, when $\sum \gamma_{ij}$ for all contacting phases i, j of a specific morphology is minimized. Again with PET (or PP) as a matrix, $\sum \gamma_{ij}$ is minimized ($\sum \gamma_{ij}^{min}$) when TPO is interposed between PET and PP. Application of this principle also excludes a morphology where all the three components are separate (see Fig. 14(b)).

For the interfacial tension calculation, the harmonic-mean equation was applied

$$\gamma_{12} = \gamma_1 + \gamma_2 - \frac{4\gamma_1^d\gamma_2^d}{\gamma_1^d + \gamma_2^d} - \frac{4\gamma_1^p\gamma_2^p}{\gamma_1^p + \gamma_2^p} \quad (2)$$

using pure component data γ_i [18,19]. In Eq. (2) indices d and p refer to the dispersive and polar component of the surface tension, respectively. Values at 280°C used in the above calculations were: $\gamma_{PP} = 15.0$, $\gamma_{PP}^d = 15.0$, $\gamma_{PP}^p = 0$ $\gamma_{PET} = 27.7$, $\gamma_{PET}^d = 21.6$, $\gamma_{PET}^p = 6.1$; $\gamma_{TPO} = 17.9$, $\gamma_{TPO}^d = 17.9$; $\gamma_{TPO}^p = 0$. Application of Eq. (2) gave, $\gamma_{PET/PP} = 7.3$, $\gamma_{PET/TPO} = 6.4$ and $\gamma_{PP/TPO} = 0.26$ dyn cm^{-1}.

For the 4-component polymer alloy, PP/PP-*g*-MA + TPO/PET, theory [17] predicts 20 possible morphologies. To arrive at a "tractable" prediction certain assumptions should be made: (i) The TPO interfaces with PET and PP as shown before; (ii) the compatibilizer is mixed with TPO. This is the result of chemical reactivity considerations since during melt-mixing MA groups react with the terminal OH of PET and a PP-*g*-PET copolymer may form [3], affecting the PET/TPO interface. In this case as well, the $\sum \gamma_{ij}^{min}$ principle proves useful in predicting most stable morphologies. One such spherical morphology is shown in Fig. 14(c) with PET as matrix. To calculate $\sum \gamma_{ij}$ one needs in addition to previous data, $\gamma_{PET/TPO}$ plus compatibilizer ($\gamma_{PET/TPO}^c$). Data on γ_{ij} in compatibilized blends are scarce. At melt-temperatures Chen and White [20] give a value of $\gamma_{PE/PA-6}^c$ and $\gamma_{PS/PET}^c$ which is about five times lower than γ_{12} in the noncompatibilized blends. In the present case, lacking relevant data, it is assumed that the

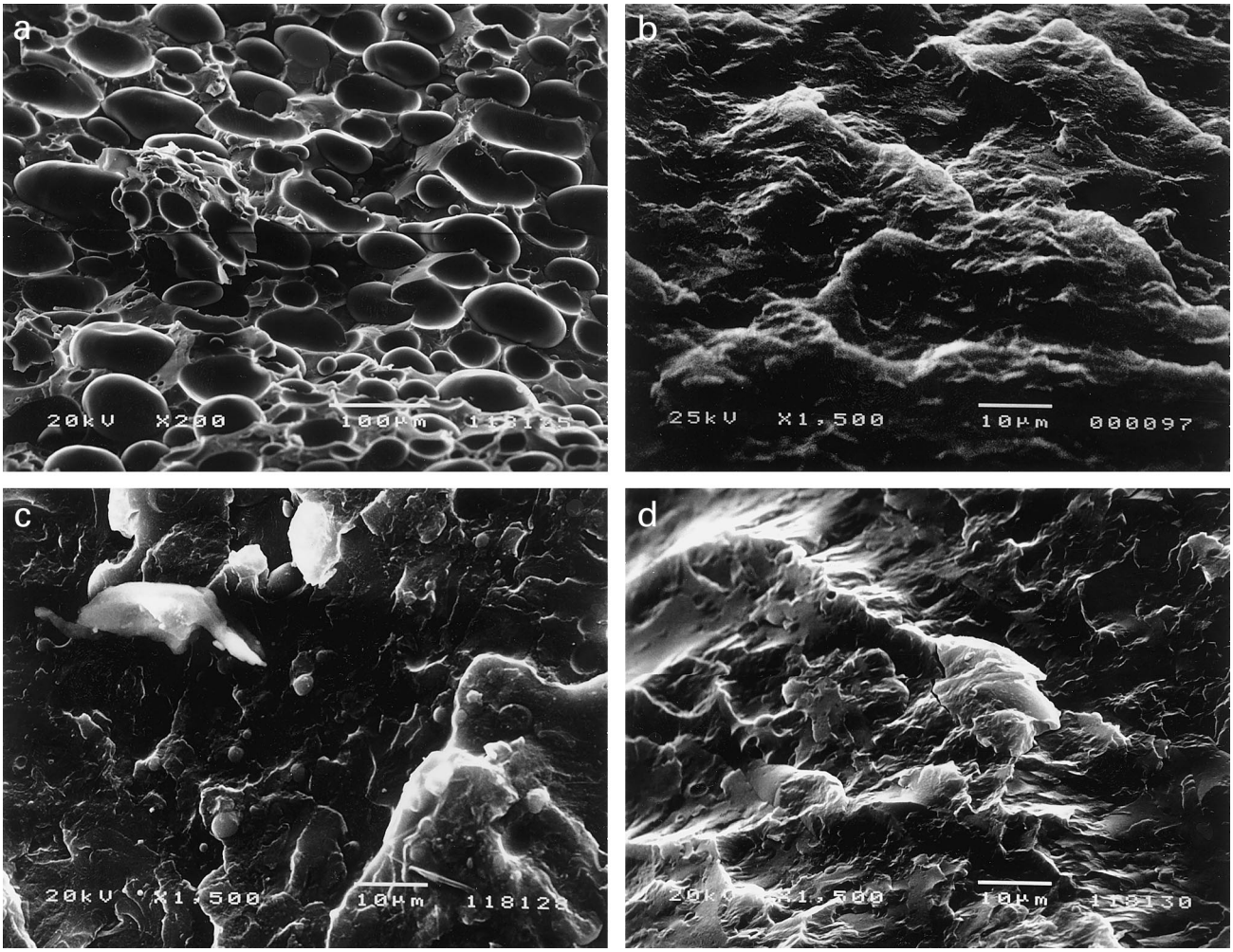

Fig. 10. SEM of cryofractured surfaces of blends: (a) PET/PP 2/1; (b) PET/SEBS-*g*-MA/PP, 56.7/15/28.3; (c) PET/PP-*g*-MA/PP, 56.7/15/28.3; (d) PET/PP-*g*-MA + TPO/PP, 53.3/15 + 5/26.7.

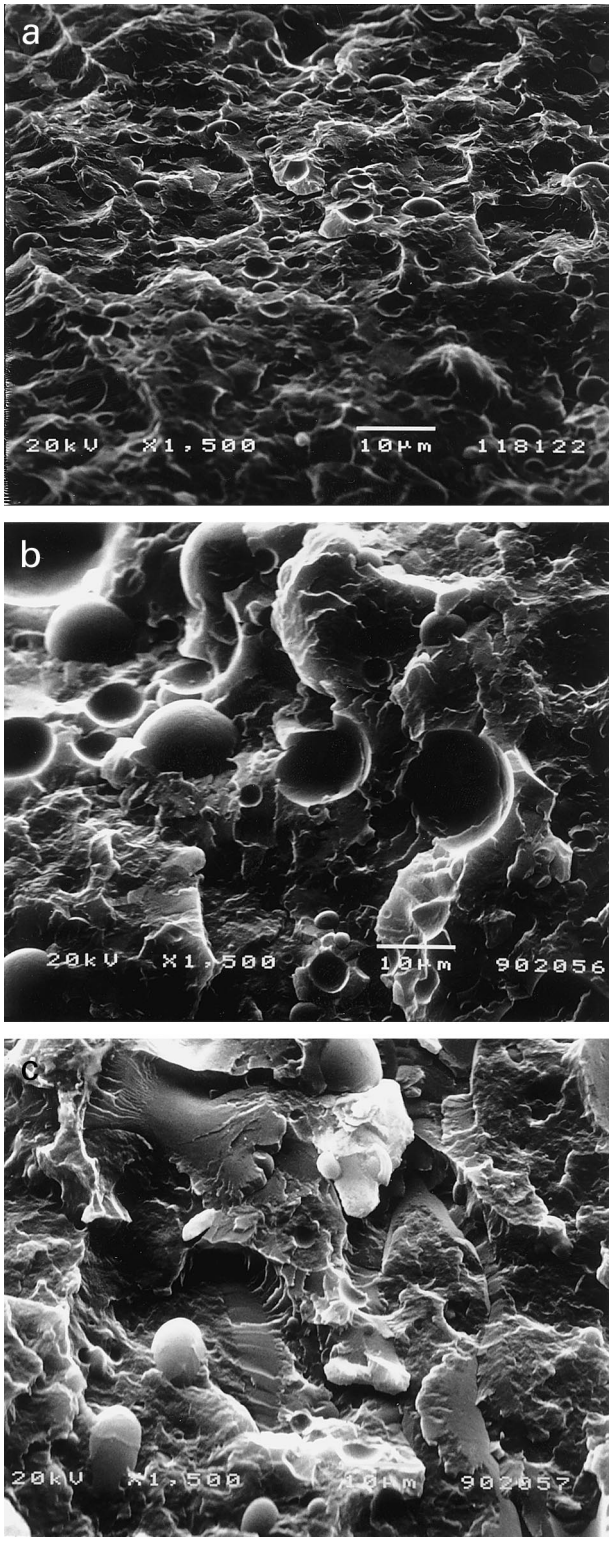

Fig. 11. SEM of cryofractured surfaces of PET/PP-*g*-MA + TPO/PP blend with varying TPO content: (a) 55.3/15 + 2/27.7; (b) 50/15 + 10/25; (c) 46.7/15 + 15/23.3.

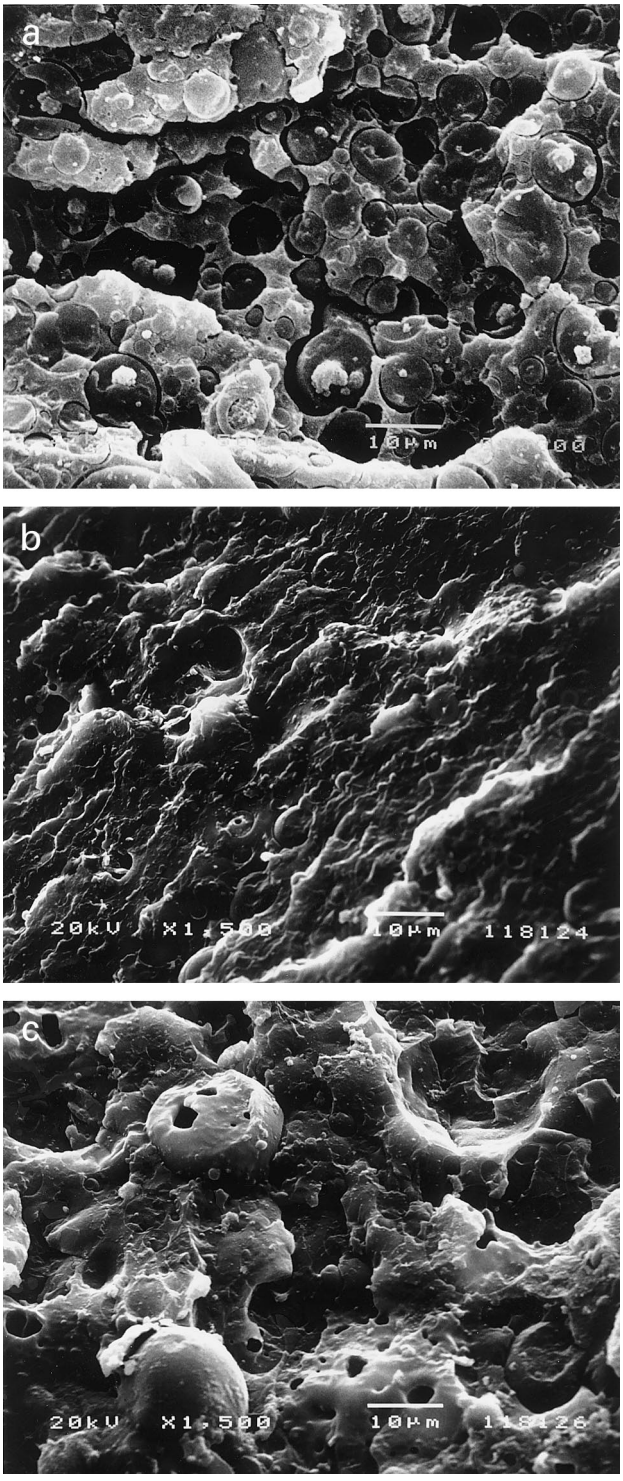

Fig. 12. SEM of cryofractured and etched blends: (a) PET/SEBS-*g*-MA/PP, 63.3/5/31.7. PET/PP-*g*-MA + TPO/PP; (b) 53.3/15 + 5/26.7; (c) 50/15 + 10/25.

compatibilizer reduces γ_{12} also by the same factor. Thus for morphology Fig. 14(c) using previous data $\sum \gamma_{ij} \cong \gamma^{c}_{PET/TPO} + \gamma_{TPO/PP} \cong 1.5$ dyn cm^{-1}. The same result is obtained with PP as matrix and PET as the dispersed phase. If PP-*g*-MA is concentrated at the PP/TPO interface and modifies $\gamma_{PP/TPO}$, (an unlikely situation), $\sum \gamma_{ij} \cong \gamma_{PET/TPO} + \gamma_{PP/TPO} \cong 6.5$ dyn cm^{-1}. An equally unstable morphology is predicted with all components

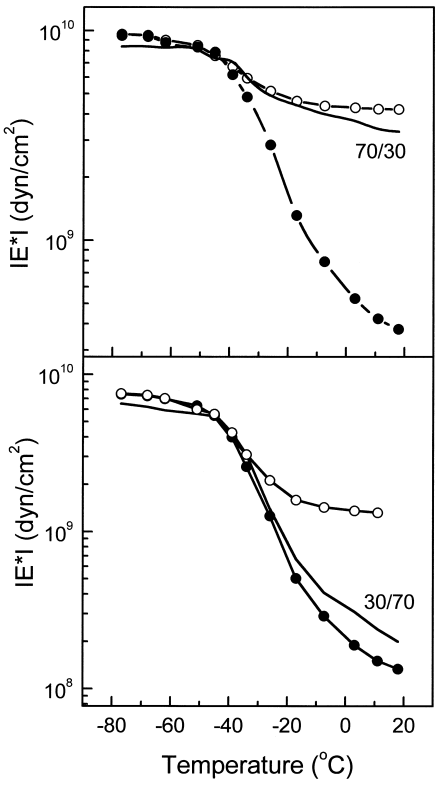

Fig. 13. Comparison of observed and calculated complex modulus $|E^*|$ of PET/SEBS-*g*-MA blends using Kerner's model at indicated compositions: (—) experimental values; calculated: (○) PET matrix, (●) SEBS-*g*-MA matrix.

forming their own separate phases as in Fig. 14(d). In this case, $\sum \gamma_{ij} \cong \gamma_{PET/PP} + \gamma_{PET/TPO} + \gamma_{PET/PP\text{-}g\text{-}MA} \cong 13.7$ dyn cm^{-1}, assuming that $\gamma_{PET/PP\text{-}g\text{-}MA} \cong 0$ dyn cm^{-1}.

Similar considerations lead one to conclude that for ternary PET/SEBS-*g*-MA/PP, a stable morphology requires that the compatibilizer interfaces between the main components.

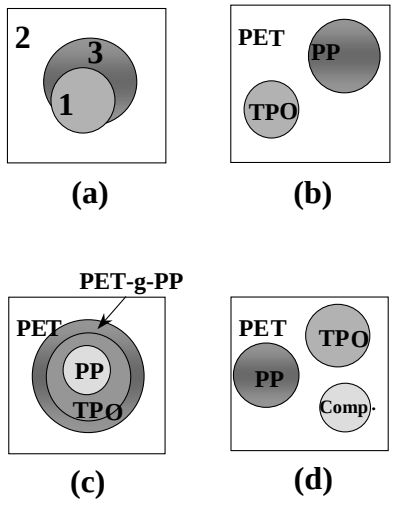

Fig. 14. Morphologies predicted by consideration of interfacial tension of PET/PP-*g*-MA + TPO/PP blends with and without compatibilizer (comp.); see text.

It should be noted that interfacial activity does not require large amount of compatibilizer. A few percent would be sufficient to improve the degree of dispersion [21]. However, in the case of reactive blending, a higher amount is required since the compatibilization reaction does not proceed to completion [22]; a broadening of the interface also takes place. Any excess of a reactive component, (unreacted SEBS-*g*-MA or PP-*g*-MA plus TPO), that cannot be "accommodated" within the interphase will phase-separate because of thermodynamic immiscibility with the matrix and by coalescence give inclusions of larger dimensions. This is supported by the morphology findings (see Fig. 7(c) and (d); Fig. 8(e) and (f); Fig. 9(e) and (f).

In addition to emulsification, concentration of the ductile TPO between PET and PP absorbs mechanical stresses developing at the interface of these hard thermoplastics. It may also interfere with PET crystallization and densification [23]. Similar findings were reported by Rösch and Mülhaupt [24,25] who compared the compatibilizing efficiency of SEBS-*g*-MA and PP-*g*-MA for PA-6/PP blends. The lower effectiveness of PP-*g*-MA was also attributed to some loss into the PP phase. In another work [26] the addition of SEBS to SEBS-*g*-MA was found to improve the toughness of PA-6/PC in addition to the compatibilization achieved. The improved performance in the presence of SEBS was attributed to its microphase domain structure and its concentration at the PA-6/PC interface enhancing its emulsifying activity.

Improvement of PA-6 toughness was also reported by Paul and coworkers [27] with the addition of MA modified ethylene–propylene copolymer or a combination of SEBS with SEBS-*g*-MA. The beneficial presence of SEBS was attributed to the size control of the dispersed elastomeric additives yielding a narrow size distribution of mixed rubber particles.

5. Conclusions

1. A comparison of the compatibilizers used for the PET/PP blend, classifies them in the following order of decreasing efficiency: SEBS-*g*-MA ≅ PP-*g*-MA + TPO ≫ LLDPE-*g*-MA ≥ PP-*g*-MA.
2. The role of the TPO in promoting the effectiveness of PP-*g*-MA is analogous to that of SEBS-*g*-MA. It relieves interfacial stresses and possibly hinders PP-*g*-MA migration into PP thus improving the efficiency of PP-*g*-MA.
3. The beneficial effect of TPO with respect to aging may be attributed to the stabilization of blend morphology and the retardation of PET crystallization and/or densification.
4. In compatibilized PET/PP alloys, the presence of PET expands the temperature range where PP stiffness is maintained.

Acknowledgements

This work was supported by the CSFII Operational Program for R&D, (subgroup 1, measure 1.4) task 623, administered by the General Secretariat of Research and Technology and coordinated by ARGO S.A., Greece. The authors are indebted to Uniroyal Chemical, Specialty Chemicals Div., UK and to Du Pont de Nemours International S.A., Switzerland, for the donation of materials and relevant information. Thanks are also due to Prof. P. Koutsoukos for the use of the SEM facility.

References

[1] Bataille P, Boissé S, Schreiber HP. Polym Engng Sci 1987;27:622.
[2] Xanthos M, Young MW, Biesenberger JA. Polym Engng Sci 1990;30:355.
[3] Sun YJ, Hu GH, Kotlar HK, Lambla M. Polymer 1996;37:4119.
[4] Ballauri B, Trabuio M, LaMantia FP. Compatibilization of recycled poly(ethylene terephthalate)/polypropylene blends using a functionalized rubber. In: LaMantia FP, editor. Recycling of PVC and mixed plastics. Toronto: Chem Tec, 1996. p. 77.
[5] Heino K, Kirjava J, Hietaoja P, Seppälä J. J Appl Polym Sci 1996;65:241.
[6] Morye SS, Kale DD. J Polym Mater 1996;13:217.
[7] Tsai CH, Chang FC. J Appl Polym Sci 1996;61:321.
[8] Zhihui Y, Yajie Z, Xiaomin Z, Jinghua Y. Polymer 1998;39:547.
[9] Carté TL, Moet A. J Appl Polym Sci 1993;48:611.
[10] Kalfoglou NK, Scafidas DS, Kallitsis JK, Lambert JC, Van der Stappen L. Polymer 1995;36:4453.
[11] Oshinski AJ, Keskkula H, Paul DR. Polymer 1996;37:4891.
[12] Papadopoulou CP, Kalfoglou NK. Polymer 1997;38:4207.
[13] Papadopoulou CP. PhD thesis, Department of Chemistry, University of Patra, 1998.
[14] Willis JM, Favis BD, Lavallée C. J Mater Sci 1993;28:1749.
[15] Kerner EH. Proc Phys Soc 1956;69B:808.
[16] Hobbs SY, Dekkers MEJ, Watkins VH. Polymer 1988;29:1598.
[17] Guo H-F, Gvozdic NV, Meier DJ. Polym Papers, Div Polym Chem 1995;36(2):120 ACS Meeting, Chicago, IL.
[18] Wu S. In: Paul DR, Newman S, editors. Polymer blends. New York: Academic Press, 1978, chap. 6.
[19] Wu S. Polym Engng Sci 1987;27:335.
[20] Chen CC, White JL. Polym Engng Sci 1993;33:923.
[21] Wu S. Interfacial and surface tension of polymer melts and liquids. New York: Marcel Dekker, 1982, chap. 3.
[22] Dedecker K, Groeninckx G, Inoue T. Polymer 1998;39:5001.
[23] Tant MR, Wilkes GL. J Appl Polym Sci 1981;26:2813.
[24] Rösch J, Mülhaupt R. Makromol Chem Rapid Commun 1993;14:503.
[25] Rösch J, Mülhaupt R. Polym Bull 1994;32:697.
[26] Horiuchi S, Matchariyakul N, Yase K, Kitano T, Choi HK, Lee YM. Polymer 1997;38:59.
[27] Oshinski AJ, Keskkula H, Paul DR. Polymer 1992;33:268.